CrossMark

Characterization of Thermal Conductivity of Carbon Fibers at Temperatures as Low as 10 K

Xuebo Liu[1] · Hua Dong[1] · Yan Li[2]

Abstract

Due to their excellent thermal structural properties, carbon fibers have been extensively applied in the fields of mechanical and aerospace engineering. Many studies have been conducted at room temperature or higher, yet the literature gives very few data on the measurement of thermophysical properties at very low temperatures. The thermal diffusivity of two kinds of carbon fibers was measured by the transient electrothermal technique at very low temperatures (down to 10 K) in the work, the ρCp followed the Debye T3 law dependence quite accurately in agreement with theoretical investigations at very low temperatures(< 10 K). The thermal diffusivity of carbon fiber almost increases linearly with decreasing temperature, but when the temperature drops down below 90 K, the thermal diffusivity rapidly decreases. The thermal expansion mismatch between the different materials present in carbon fibers may influence the change of thermal diffusivity. The relationship between the impurity concentration and the thermal transport of the carbon fibers is discussed.

1 Introduction

Due to their excellent thermal structural properties, carbon–carbon composites are used in specialized applications such as aircraft/aerospace engines, Formula 1 motor brakes and clutches, in addition to several industrial and biomedical applications. The

✉ Yan Li
  yanli@ouc.edu.cn

1 School of Environmental and Municipal Engineering, Qingdao University of Technology, Qingdao 266033, Shandong, People's Republic of China

2 College of Engineering, Ocean University of China, Qingdao 266100, Shandong, People's Republic of China

thermal conductivity and thermal expansion of carbon fibers (CFs) are significant important properties in the study of carbon–carbon composites.

Some data on the thermophysical properties of CFs at very low temperatures can be found in the literature [1]. Due to the microscale of the fibers ($\approx 10\ \mu m$ in diameter) and the extremely low temperature, measuring CF's thermophysical properties at temperatures as low as 10 K is difficult. The transient electrothermal (TET) technique was often used to determining the thermophysical properties of micro/nanoscale materials in a low temperature range (i.e., 10 K to 300 K).

The aim of the study is to present how the thermal diffusivity of CFs varies with temperature by measuring the longitudinal thermal diffusivity at different temperatures. With the calibration result of the resistance change ΔR and temperature change ΔT during the cooling process, then the thermal conductivity can be obtained (Eq. 1), where L and A are the length and area of cross section of the sample [2]. Meanwhile, the volume-based specific heat of CF (ρCp) can be calculated (Eq. 2) with the thermal diffusivity (α) obtained from transient process and the thermal conductivity (k) obtained from Eq. 1.

$$k = \frac{I^2 R L}{12 A \Delta T} \tag{1}$$

$$k = \alpha \rho C p \tag{2}$$

In Sect. 2, the materials and structures are characterized by X-ray photoelectron spectroscopy (XPS) and Raman spectroscopy. The thermal characterization method is presented in Sect. 3.

2 Structural Analysis and Measurement

2.1 Structural Properties

In the study, two kinds of carbon fibers were measured. Samples A and B were obtained from Jiangsu Hengshen Corporation and Beijing Terminate Technology Development Co., Ltd., respectively. Figure 1a, b shows the scanning electron microscope (SEM) images of CF samples with high magnification, where the surface structure can be clearly seen. The measured diameter is about 7.61 $\mu m \pm 0.03\ \mu m$ and 8.54 $\mu m \pm 0.01\ \mu m$, respectively.

Figure 2 compares the 532 nm Raman spectra of samples A and B. The main features in the Raman spectra of CFs are the D, G, and 2D peaks, which appear around 1352 cm^{-1}, 1594 cm^{-1}, and 2700 cm^{-1}, respectively. The intensity of the D peak is inversely proportional to the crystallite grain size, and its appearance is related to the occurrence of defects and disorder in general. The G peak is caused by the Raman-active E_{2g} phonon, which is present in all of the graphite and graphene samples studied [3–5]. The 2D peak is caused by the second-order zone-boundary phonons. However, the zone-boundary phonons do not satisfy the Raman fundamental selection rule, so the 2D band does not appear in the Raman spectrum of sample A. The ratio of the
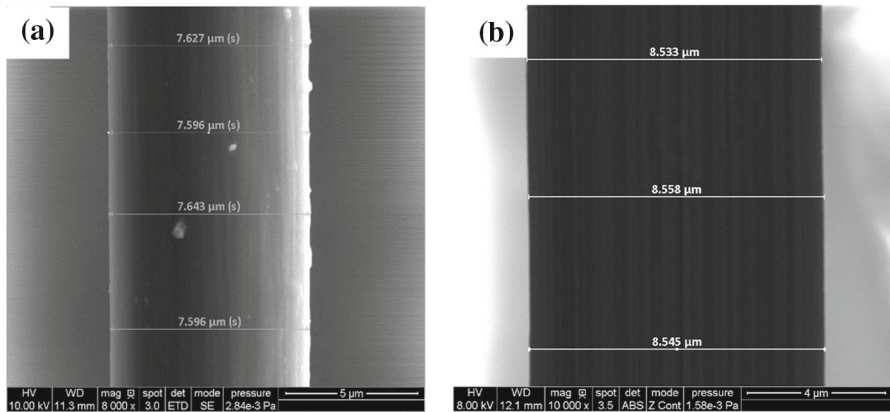
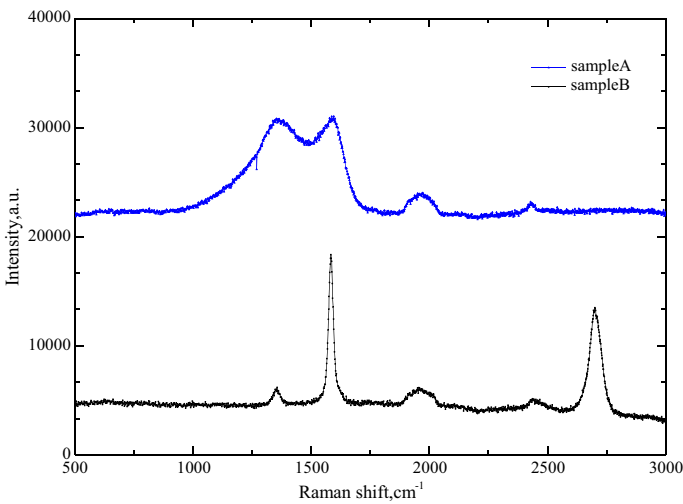**Fig. 1** SEM images of the two kinds of CF samples studied in this work

Fig. 2 Raman spectra of the CF samples collected at the same conditions: continuous-wave laser at a wavelength of 532 nm, a × 50 lens, an integration time of 10 s, and a laser energy of 3.5 mW

Table 1 XPS results of the two CF samples

	Carbon (%)	Oxygen (%)	Nitrogen (%)	Silicon (%)
Sample A	78.4	18.2	1.57	1.8
Sample B	90.3	7.5	0.8	1.41

integrated intensities of the G band and 2D band (I_G/I_{2D}) was determined to be 0.48, which can be used to obtain the number of layers of graphene [4].

Table 1 shows the XPS results of the two CF samples, indicating the higher content of impurities in sample A.
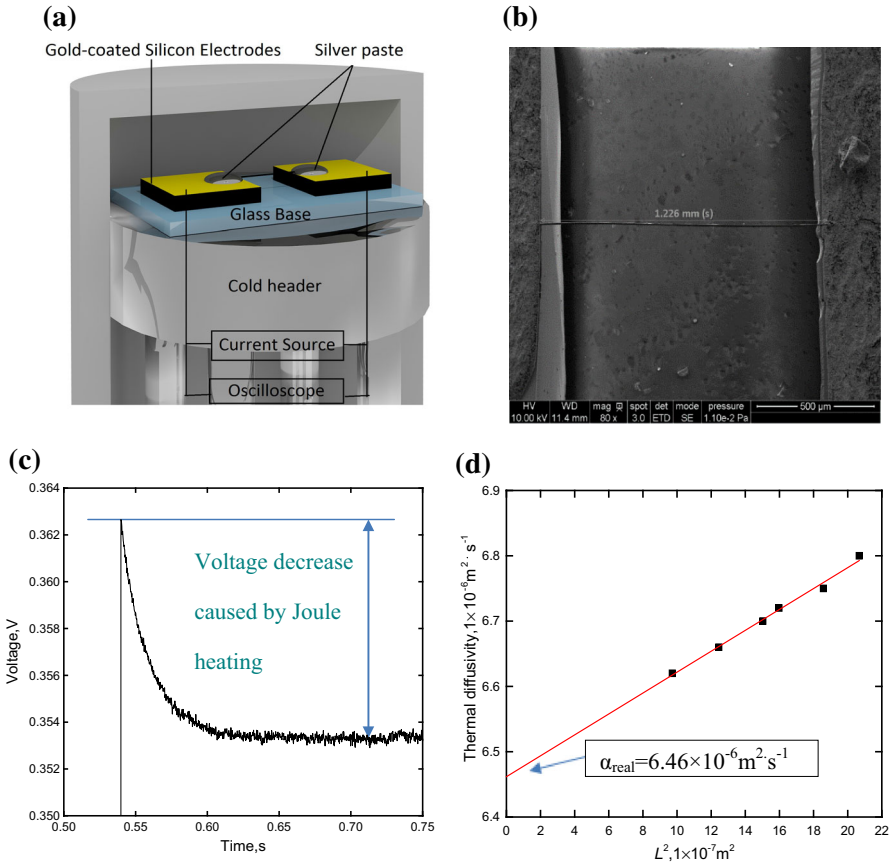
(a)

(b)

(c)

(d)

Fig. 3 (a) Schematic of the TET setup for data collection. (b) SEM image of the CF sample (sample A). (c) The V–t data of sample A collected by the digital phosphor oscilloscope. (d) Linear fitting (solid line) of the thermal diffusivity of sample A

2.2 Measurement Principle

The thermal diffusivity of the CF samples at different temperatures was measured by the TET technique. The schematic and principles of the TET experiment can be found in Ref. [6, 7].

A cryogenic system (CCS-450, Janis) was used to provide a stable and reliable environmental temperature in the process of experiment. The sample to be measured was suspended between two electrode substrates and put into a cryogenic system, which is shown in Fig. 3a. In order to eliminate the effects of heat convection on the experiment, a liquid nitrogen cold-trapped mechanical vacuum pump was used to keep the vacuum level under 0.5 mTorr.

The thermal diffusivity measured by the TET experiment includes the real thermal diffusivity and the radiation effect:

$$\alpha_{measure} = \alpha_{real} + \frac{16\varepsilon\sigma L^2 T^3}{D\pi^2 \rho Cp} \tag{3}$$

In the above definition, ε, σ and ρCp are the emissivity, Stefan–Boltzmann constant diameter and specific heat, respectively.

A digital phosphor oscilloscope was used to record the voltage–time (V–t) profile at intervals of 20 K in the range of 290 K to 100 K. From 100 K down to 10 K, more data points were recorded at intervals of 10 K to get a clearer view. Figure 3c presents a typical V–t profile. The temperature increase caused by Joule heat will lead to decrease in the resistance of CF. There have a linear relationship between the sample's resistance and its average temperature [8], which linearly reflects in the decreasing voltage. Through fitting the V–t data, we can obtain the thermal diffusivity of CF.

3 Results and Discussion

3.1 Measurement of the Thermal Diffusivity

First, the sample A at room temperature (290 K) was used as an example to describe how the thermal diffusivity is characterized. Figure 3b shows the length of sample measured under the SEM. The length and diameter of this sample are 1226 and 7.62 μm ± 0.03 μm, respectively. Figure 3c shows the raw experimental data of CF when the transient voltage changes. Before feeding the step dc current through the sample, the measured voltage is 2.67×10^{-1} V. While as the step dc current is applied, the induced voltage begins to decrease and finally reaches a steady state at about 2.63×10^{-1} V. The thermophysical properties of the CF sample and its length will strongly affect the time to reach a steady state [6, 9]. In order to get more accurate result, the same sample was measured with different currents several times.

In Eq. 3, the real thermal diffusivity (α_{real}) increases linearly with the square of length (L^2). The thermal diffusivity of CF with different lengths was measured by the TET experiment to eliminate the radiation effect. Figure 3d shows the linear fitting results of $\alpha_{measure}$ vs. L^2 for sample A with different lengths at room temperature. Extrapolating the linear plots of α–L^2 to the y-axis yields a y-intercept value of 6.46×10^{-6} m^2 s^{-1}, which represents the $\alpha_{measure}$ value of the CF sample without the radiation effect (i.e., α_{real}) [10].

Here using the slope of fitting line, the emissivity of CF sample is calculated (Eq. 4) as 0.78 which can be used to subtract the effect of radiation on thermal diffusivity at other temperature [10].

$$\varepsilon = \frac{\psi D\pi^2 \rho Cp}{16\delta T^3} \tag{4}$$

3.2 Variation in the Thermal Properties as a Function of Temperature

Figure 4d shows the relationship between resistance and temperature and it can be used to calculate the thermal conductivity. Figure 4c shows the relationship of thermal
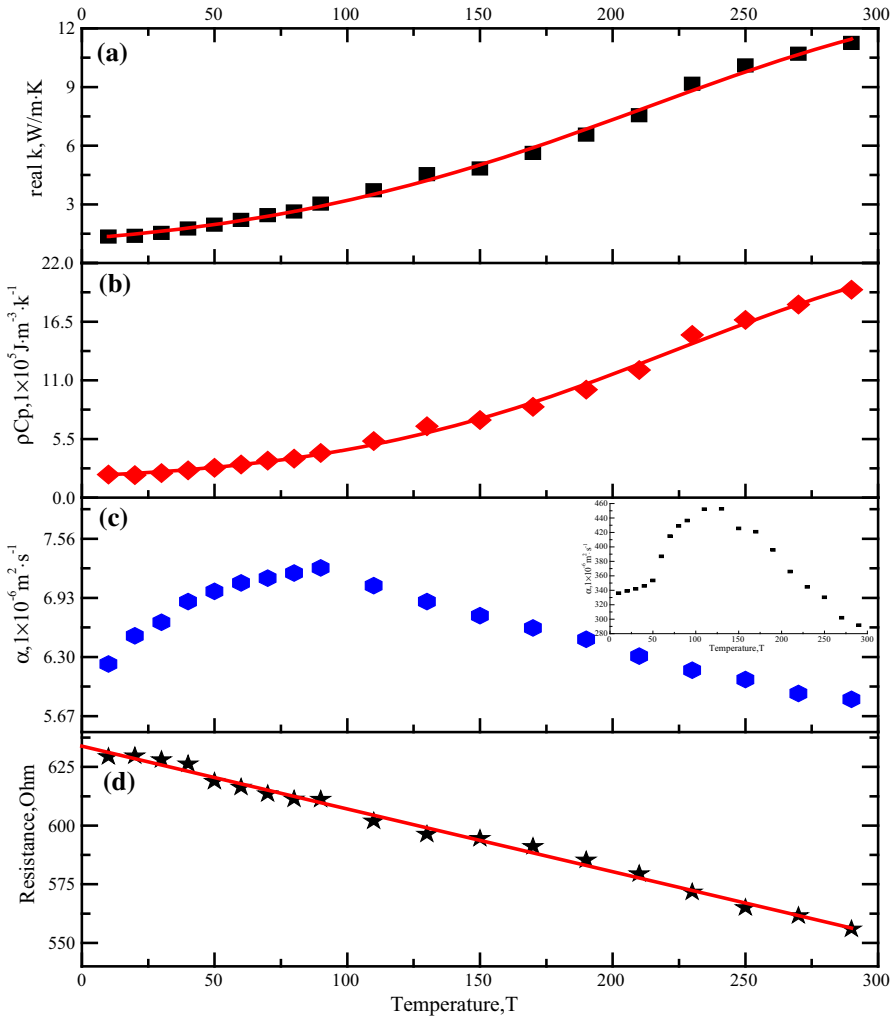
Fig. 4 (a) The real thermal conductivity as a function of temperature T and (b) The specific heat of CFs per unit volume (ρCp). (c) The real thermal diffusivity α_{real} plotted against temperature T. α_{real} increases approximately linearly with temperature when the temperature decreases from 290 K to 90. But when the temperature drops down below 90 K, α_{real} exhibits a sharp turning point and then decrease rapidly. The inset demonstrates the $\alpha_{real}-T$ curve of sample B. (d) The relationship between resistance and temperature of sample A

diffusivity vs. temperature (α–T) for sample A, wherein α_{real} increases as the temperature decreases from 290 K to 90 K. This means that heat transfers faster in CFs at lower temperatures. The temperature-dependent change in the phonon scattering mechanism of the material will affect the thermal diffusivity of CFs. With microscale changes in the physical structure, α_{real} tends to decline rapidly when the temperature decreases from 90 K to 10 K.

Specific heat is the amount of heat needed to raise the temperature of one kilogram of mass by 1 K. According to the Debye model, the specific heat can be described as: $Cp = 9Nk_B \frac{T^3}{\theta_D^3} \int_0^{\frac{\theta_D}{T}} \frac{x^4 e^x}{(e^x-1)} dx$ and $x = \frac{\hbar\omega}{k_b T}$ where N is Avogadro constant, k_B is Boltzmann constant, T is the thermodynamic temperature, θ_D: $\hbar\omega_D = k_B \theta_D$ is the Debye temperature, $\hbar$ is Planck's constant, ω_D is cutoff frequency for each phonon branch. At the extreme low temperature, $x \gg 1$, $\theta_D/T \to \infty$, then got: $Cp = \frac{12\pi^4}{5} Nk_B \left(\frac{T}{\theta_D}\right)^3$, which indicates that the low temperature dependence of the specific heat (heat capacity) in solid follows the T^3 law. As the temperature approaches absolute zero, the specific heat of a material is close to zero. It is common knowledge that there isn't any experimental data for the specific heat of CF at extreme low temperature. The specific heat of CF per unit volume (ρCp) can be calculated (Eq. 2). Figure 4c presents the volume-based specific heat of CF (ρCp) variation against temperature.

The calculated thermal conductivity with the measured thermal diffusivity and the calculated specific heat are also in good agreement with references [11, 12]. The real thermal conductivity plotted (k_{real}) against temperature (Fig. 4d) decreases as T decreases from 290 K to 50 K. In addition, it tends to stabilize when the temperature decreases from 50 K to 10 K.

3.3 Physics Underlying the Thermal Conductivity

From Fig. 2, the ratio of the intensity of D peak to that of G peak (I_D/I_G) is 0.98, indicating greater disorder in the tested CF sample A. The ratio was firstly used by Heremans et al. [11] to measure the ratio of the intensity of disorder induced to Raman-allowed lines. In perfect graphite and graphene, the ratio is close to zero.

In a solid, there exists two mechanisms which contribute to thermal conduction: the first is via electrical conductivity and the second is by lattice vibrations. In graphite, atoms are kept together by a mixture of sp^2 δ and π bonding. These layers of graphite are very loosely combined through weak van der Waals' forces. For no electron moves between the layers, the effect of electrical conductivity to the thermal conductivity of graphite is negligible [13]. Phonons sustains the thermal conductivity mechanism in CFs, and the thermal transport is dominated by phonon scattering. The Phonon scattering exhibits several mechanisms: collision with other phonons, collision with lattice defects, crystal boundaries or pores. At or above room temperature, the carriers in carbon-based materials are mainly subjected to phonon scattering. At a specific temperature, the number of phonons participating in thermal transfer can be depicted by the Bose–Einstein distribution $n = \frac{1}{e^{\hbar\omega/Tk_B}-1}$ [14], where $\hbar$ is Planck's constant and k_B is Boltzmann constant. According to the Debye model, when the temperature (T) is below the Debye temperature (θ_D), the energy of phonon is $k_B\theta_D/2$. Thus, we have: $n \approx \frac{1}{e^{\theta_D/2T}-1} \approx e^{-\frac{\theta_D}{2T}}$. As the temperature decreases, lattice vibrations weaken, and the number of phonon scattering decreases, which makes the thermal diffusivity to increase [15].

For one-dimensional molecular structures, the thermal conductivity can be described as $k = \rho C p v l_{eff}/3$, where $\rho C p$ is the volume-based specific heat, v is the average velocity of all phonons in the Brillouin zone, which is independent of temperature, and l_{eff} is the mean free path of phonons. The mean free path includes the effect of all phonon scattering mechanisms and phonon collision, and it can be written according to Matthiessen's rule as $l_{eff}^{-1} = l_0^{-1} + l_i^{-1}$, where l_0 and l_i are the mean free path due to collision with other phonons and the mean free path due to defect-induced scattering, respectively. When the temperature drops below the Debye temperature, the collision with other phonons becomes so weak that the mean free path of the phonon is determined by the length and defect level of sample, which is close to a nonzero value and the thermal conductivity is a nearly constant.

CFs are a mixture of a well-ordered material surrounded by disordered and impure materials. The CF sample contains other elements (oxygen, nitrogen, and silicon) whose coefficients of thermal expansions (CETs) are different from that of carbon [16, 17]. When the temperature decreases to 90 K and lower, these materials can exhibit thermal expansion mismatch with carbon, which leads to the change in the relationship between the well-ordered and disordered materials. These changes result in the rapid decrease in the thermal diffusivity.

4 Conclusion

In the work, the thermal diffusivity and conductivity of CFs from 290 K to 10 K were characterized by the TET technique. Meanwhile, the relationships between the specific heat of CFs per unit volume ($\rho C p$) and temperature were also characterized. The thermal transport is dominated by phonon scattering in CFs. As the temperature decreases, the phonon scattering by carriers weakens, which results in increasing thermal diffusivity. The XPS results reveal the chemical composition of carbon, oxygen, nitrogen, and silicon. Due to the different CETs, the relationship between these elements and the carbon in CFs changes with the decreasing temperature, which results in the rapid decrease in the thermal diffusivity as the temperature decreases to 90 K.

References

1. B. Nysten, L. Piraux, J.P. Issi, J. Phys. D Appl. Phys. **18**, 1307 (1985)
2. X. Feng, X. Wang, X. Chen, Y. Yue, Acta Mater. **59**, 1934 (2011)
3. A.C. Ferrari, Solid State Commun. **143**, 47 (2007)
4. D. Graf, F. Molitor, K. Ensslin, C. Stampfer, A. Jungen, C. Hierold, L. Wirtz, Nano Lett. **7**, 238 (2007)
5. M.A. Pimenta, G. Dresselhaus, M.S. Dresselhaus, L.G. Cançado, A. Jorio, R. Saito, Phys. Chem. Chem. Phys. **9**, 1276 (2007)
6. J.Q. Guo, X.W. Wang, T. Wang, J. Appl. Phys. **101**, 063537 (2007)
7. G.Q. Liu, H. Lin, X.D. Tang, K. Bergler, X.W. Wang (2014). https://doi.org/10.3791/51144
8. J. Guo, X. Wang, D.B. Geohegan, G. Eres, C.C. Vincent, J. Appl. Phys. **103**, 113505 (2008)
9. J.Q. Guo, X.W. Wang, L.J. Zhang, T. Wang, Appl. Phys. A Mater. **89**, 153 (2007)

10. X. Liu, H. Dong, Y. Li, N. Mei, Int. J. Thermophys. **38**, 150 (2017)
11. J. Heremans, I. Rahim, M.S. Dresselhaus, Phys. Rev. B **32**, 6742 (1985)
12. C. Pradere, J.C. Batsale, J.M. Goyhénèche, R. Pailler, S. Dilhaire, Carbon **47**, 737 (2009)
13. H. Lin, S. Xu, Y.Q. Zhang, X.W. Wang, ACS Appl. Mater. Interfaces. **6**, 11341 (2014)
14. C. Kittel, *Introduction to Solid State Physics*, 5th edn. (Wiley, New York, 1971), p. 171
15. Y.S. Xie, Z.L. Xu, S. Xu, Z. Cheng, N. Hashemi, C. Deng, X.W. Wang, Nanoscale **7**, 10101 (2015)
16. C.H. Xu, C.Z. Wang, C.T. Chan, K.M. Ho, Phys. Rev. B **43**, 5024 (1991)
17. P.K. Schelling, P. Keblinski, Phys. Rev. B **38**, 521 (1985)